Characterization and Use of a Fiber Optic Sensor Based on PAH/SiO2 Film for Humidity Sensing in Ventilator Care Equipment

Article *in* IEEE Transactions on Biomedical Engineering · February 2016

DOI: 10.1109/TBME.2016.2521662

CITATIONS
6

READS
103

9 authors, including:

Francisco Ulises Hernandez Ledezma
University of Nottingham
10 PUBLICATIONS **27** CITATIONS
SEE PROFILE

Andrew Michael Norris
University of Nottingham
37 PUBLICATIONS **414** CITATIONS
SEE PROFILE

Jonathan G Hardman
University of Nottingham
196 PUBLICATIONS **1,539** CITATIONS
SEE PROFILE

Sergiy Korposh
University of Nottingham
81 PUBLICATIONS **534** CITATIONS
SEE PROFILE

Characterisation and Use of a Fibre Optic Sensor based on PAH/SiO_2 Film for Humidity Sensing in Ventilator Care Equipment

Francisco U. Hernandez, Stephen P. Morgan, Barrie R. Hayes-Gill, Daniel Harvey, William Kinnear, Andrew Norris, David Evans, Jonathan G. Hardman and Sergiy Korposh*

***Abstract*— *Objective*: To develop a compact probe that can be used to monitor humidity in ventilator care equipment. A mesoporous film of alternate layers of Poly(allylamine hydrochloride) (PAH) and silica (SiO_2) nanoparticles (bilayers), deposited onto an optical fibre was used. The sensing film behaves as a Fabry-Perot cavity of low-finesse where the absorption of water vapour changes the optical thickness and produces a change in reflection proportional to humidity. *Methods*: The mesoporous film was deposited upon the cleaved tip of an optical fibre using the layer-by-layer method. The sensor was calibrated in a bench model against a commercially available capacitive sensor. The sensitivity and response time were assessed in the range from 5 % relative humidity (RH) to 95 %RH for different numbers of bilayers up to a maximum of nine. *Results*: The sensitivity increases with the number of bilayers deposited; sensitivity of 2.28 mV/%RH was obtained for nine bilayers. The time constant of the response was 1.13 s ± 0.30 s which is faster than the commercial device (measured as 158 s). After calibration, the optical fibre humidity sensor was utilised in a bench top study employing a mechanical ventilator. The fast response time enabled changes in humidity in individual breaths to be resolved. *Conclusion*: Optical fibre sensors have the potential to be used to monitor breath to breath humidity during ventilator care. *Significance*: Control of humidity is an essential part of critical respiratory care and the developed sensor provides a sensitive, compact and fast method of humidity monitoring.**

***Index Terms*—Humidity sensor, relative humidity, Fabry-Perot, layer-by-layer (LbL), intensive care unit, critical care, optical fibre sensor.**

This work was supported by National Institute of Health Research, Invention for Innovation programme (NIHR i4i II-LA-0813-20008), UK. FUH was supported by a scholarship from CONACYT and the Ministry of Education of Mexico (DGRI-SEP).

FUH, SPM. BRHG, SK are with the Advanced Optics Group, Faculty of Engineering, University of Nottingham, UK (e-mail: francisco.hernandez@nottingham.ac.uk, steve.morgan@nottingham.ac.uk, barrie.hayes-gill@nottingham.ac.uk, s.korposh@nottingham.ac.uk). WK is with the Respiratory Medicine department, and DH, AN, DE and JGH are with the Anaesthesia & Critical Research Group, Nottingham University Hospital NHS Trust, UK (emails: william.kinnear@nuh.nhs.uk, daniel.harvey@nuh.nhs.uk, andrew.norris@nottingham.ac.uk, daveevans@doctors.net.uk, j.hardman@nottingham.ac.uk).

I. Introduction

HUMIDIFICATION of inspired gases is an essential part of the clinical treatment in critical respiratory care, and inhalation of inadequately humidified gas during invasive (through a endotracheal tube (ETT) placed in the patient's trachea) or non-invasive (via a mask placed on the patient's face) ventilation causes drying of the delicate respiratory mucosa and consequent cooling, mucosal injury, drying of (and difficulty clearing) secretions and respiratory deterioration [1]. The human airway has the role of heating and humidifying inspired gas, and recovering heat and moisture from expired gas [2]. Water can exist in two forms when carried in gas: "moisture" is water in liquid form that is suspended in a gas in the form of small droplets, and "humidity" is water vapour (i.e. in gas phase) [3]. Humidity can be described as "absolute" or "relative": *absolute humidity* (AH) is the mass of water vapour in a given volume of gas, while *relative humidity* (RH) is the amount of water vapour present in a gas as a percentage of the saturated vapour pressure capacity [1], [2].

The clinically acceptable range of AH and RH values at the level of the upper trachea is between 5 mg/L (50% RH at 27 - 28 ℃) and 42 mg/L (85% RH at 34 ℃ nasal, 95% RH at 35 ℃ naso/oropharynx) [4]. Levels of AH lower than 5 mg/L represent a significant risk of respiratory complications related to inadequate humidification of inspired air. Under typical conditions in-vivo, end-inspiratory and end-expiratory values of AH are between 15 mg/L and 37 mg/L at temperatures between 28 ℃ and 34 ℃ [5]. It has been demonstrated that using an appropriate humidification system, AH values between 25 and 30 mg/L are adequate for the physiological functioning of the upper airway [2].

During invasive mechanical ventilation (where the oro/nasopharynx is bypassed and native humidification is prevented), it is recommended that AH of inspired gas should be from 33 mg/L to 44 mg/L and gas temperature should be between 34 to 41 ℃ (i.e. RH 100%) to avoid time-dependent injury to epithelial cells in the airways, and thus maintain normal mucociliary function [6]. In addition, there is a correlation between humidification and ventilator associated pneumonia (VAP) risk, and higher levels of humidity to the airway (44 mg water vapour/L gas) can facilitate maximal

mucociliary clearance [7].

Currently, during prolonged invasive mechanical ventilation, respiratory gases are actively humidified by means of a heated water bath in order to achieve levels of humidity approaching 100% RH. Gases are kept warm in the inspiratory limb of respiratory tubing in order to reduce condensation. However, due to the limitations of current humidity sensors, humidity is not actually measured at the patient end of the circuit or inside the patient's airway.

An optical fibre based humidity sensor has a potential application in this setting. Fibres are advantageous due to their light weight, simple configuration, small size, high sensitivity, efficiency and resolution. They carry no electric current, are biocompatible and potentially inexpensive optical sensors that have been demonstrated to be the fastest humidity sensors [3], [8]. There are a number of practical ways for building up optical fibre sensors to detect humidity such as evanescent wave monitoring, in-fibre gratings (fibre Bragg grating and long period grating) techniques, interferometric approaches, hybrid sensors (grating + interferometric) and absorption measurements [3], [9]. In the research described here, the goal is to develop an optical fibre Fabry-Perot interferometric sensor to detect humidity by increasing sensitivity through the deposition of a hydrophilic coating material on the cleaved distal optical fibre tip (forming a Fabry-Perot cavity). In comparison to other sensing techniques, the interferometric approach proposed in this work has the advantage of simple configuration, small size probe (125 μm) and low cost manufacture. On exposure of the hydrophilic film to a humid environment, the water vapour is absorbed, changing the effective refractive index and thickness of the film, inducing a change in the overall reflection [8].

The total reflection intensity due to the Fabry-Perot cavity created by the film deposited onto the tip of the fibre can be explained as follows: 1) the presence of two optical interfaces (fibre-film and film-air), each with its characteristic Fresnel coefficients for reflection, leads to a division of the incident beam into two main back reflections (higher-order reflections between the interfaces can be neglected), and the optical fibre sensor behaves as a Fabry-Perot interferometer of low finesse [10],[11]; 2) loss factors and coefficients associated with losses are due to optical absorption and scattering of the beam by interfaces and film itself; 3) changes in total optical reflection are due to changing the optical thickness of the film (the product $\eta_f * L$). The reflection spectrum will change when the geometrical thickness (L) increases by means of either the number of film layers deposited on the tip or the swelling due to water absorption [8]. The response in the total optical intensity reflected can also be modulated by adsorption and absorption of water vapour molecules by means of changing the effective refractive index of the film (η_f), following the Bruggeman effective medium model criteria [11].

Corres et al. [12] first demonstrated a humidity sensor at the tip of an optical fibre based on a multilayer hydrophilic film comprised of layers of SiO_2 nanoparticles with alternating pH. Through tests conducted using a humidity chamber, the sensor was demonstrated to have low hysteresis and fast response time. A simple experiment of monitoring 3 breaths on the sensor indicated potential for breathing rate monitoring.

In this work, a sensor probe film has been developed by depositing alternate layers of Poly(allylamine hydrochloride)(PAH) and silica nanoparticles (SiO_2, diameter between 40 nm and 50 nm) on the cleaved tip of an optical fibre coupler. In contrast to Corres et al. [12], this work uses PAH, a highly hydrophilic polycation layer, to assemble a SiO_2 thin film. The PAH layer increases the sensitivity of the sensor due to high hydrophilicity and also reduces the number of the deposited layers, thus increasing the efficiency of the fabrication procedure. Furthermore, after calibration, the performance of the sensor is demonstrated in a bench top study implementing a humidifier and a mechanical analogue of the respiratory system which is conventionally used for teaching and research [13] thus allowing investigation of its potential use in critical care conditions.

II. Methods

A. Materials

Poly(allylamine hydrochloride) (PAH, M_W:~58,000), NaOH, KOH and ethanol were purchased from Sigma-Aldrich, UK. Silica nanoparticles (SiO_2, SNOWTEX 20L, diameter 40 nm to 50 nm) were obtained from Nissan Chemical, Japan. All reagents were of analytical grade and used without further purification. Distilled water (18.3 MOhm cm) was obtained by reverse osmosis followed by ion exchange and filtration in a Millipore-Q (Millipore, Direct-QTM).

B. PAH/SiO_2 film deposition

The method of deposition of the nano-thin film followed the steps depicted in Fig. 1 as follows: (i) treatment of the surface-tip of the fibre with 1 wt% ethanolic (H_2O:ethanol=3:2) KOH for 20 min to terminate it with OH groups; (ii) wash with deionized water and dry with nitrogen, followed by immersion of the fibre tip in 0.17 wt% of positively charged polymer PAH (pH=11) for 15 min; (iii) wash and dry, immerse the fibre tip into a solution containing negatively charged SiO_2 nanoparticles for 15 min; (iv) after deposition of the SiO_2 nanoparticles, wash and dry and repeat steps (ii) and (iii) "X" times in order to build up an "X" layer film (denoted as $(PAH/SiO_2)_X$).

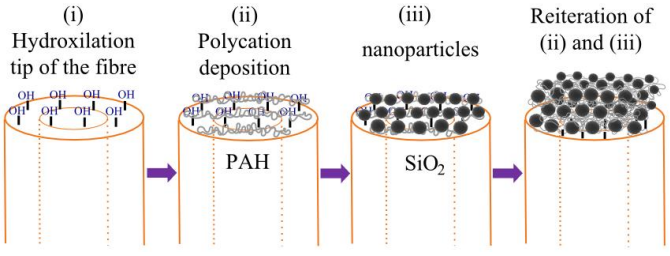

Fig. 1. Schematic representation of the construction of a (PAH/SiO_2) thin film using the Layer-by-Layer method.

C. Humidity sensor calibration

Fig. 2(a) presents the experimental set up for humidity calibration measurements. The sensor probe (tip of port1, Fig. 2(b)) and a commercial capacitive sensor (Maxim Integrated, DS1923, RH range of 0% to 100%; accuracy ± 5% in the range of -20 ℃ to +85 ℃, resolution 0.04%RH in 16-bit mode) were placed 1 cm apart in a measuring cell (200 ml). The cell receives either humidified (via flowmeter F1, Cole-Parmer, OU-32460-42, range 0 L/min to 1 L/min) or dried (via flowmeter F2) gas through the circuit. The rate of flow via the gas inlet (*L*) was a constant (1 L/min) and the flowmeters enabled different levels of humidification. Fibre tips with different numbers of layers were tested in order to ascertain the most sensitive response to humidity. The fibre coupler received light from a tungsten-halogen lamp (Ocean Optics, HL-2000, which covers the visible spectrum with an output light stability of 0.15% peak-to-peak and an optical output drift < 0.3% per hour) into port 2 of the fibre; there were reflections at the tip of the port 1 and the reflected light was collected using the CCD spectrometer (Ocean Optics, HR4000) through port 3. A spectrometer was used in order to ascertain the optimum wavelength at which to monitor intensity changes.

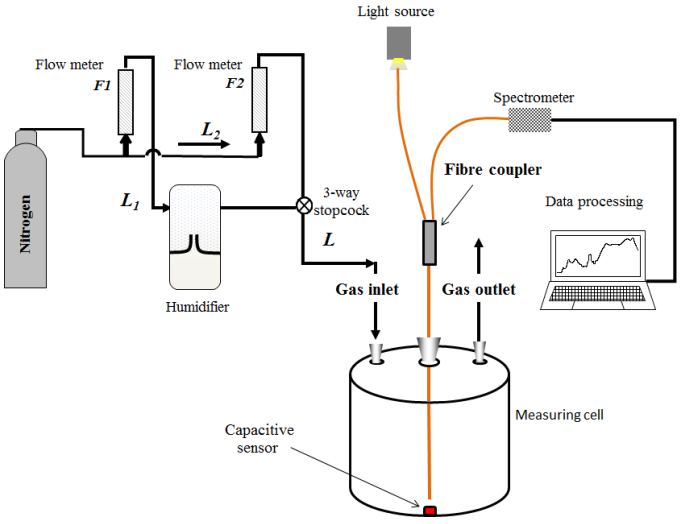

Fig. 2. (a) Humidification system to calibrate the optical fibre humidity sensor against a capacitive sensor. (b) Schematic illustration of the ports of the fibre coupler.

D. Humidity sensor response time

Fig. 3 depicts the experimental set-up used to measure humidity response time constant. The optical fibre humidity probe was inserted into and extracted from the headspace of a Petri dish (65 ml) containing 10 ml of water. The fibre was contained inside a 23-gauge medical hypodermic needle in order to provide mechanical protection for the thin film. The petri dish was closed until the humidity measured using the capacitive sensor inside the petri dish stabilised (92%RH). The external capacitive sensor monitored room humidity (42 %RH).

The experimental procedure for determining the humidity response time constant used by the manufacturer of the capacitive sensor was followed in order to make comparison with the optical fibre device. The average 1/e point as the sensor response transitions from 90% RH to 40% RH (in this case from 92% RH to 42% RH) at equilibrium conditions and constant temperature (in this case T=21.4 ± 0.2 ℃) was obtained by inserting and extracting the optical fibre humidity probe five times from the Petri dish.

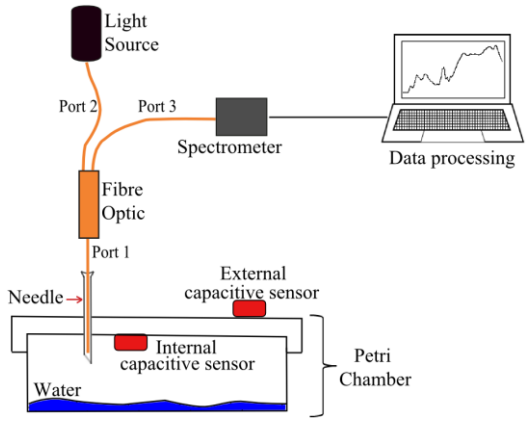

Fig. 3. Set-up to measure the humidity response time constant.

E. Sensor testing in a breathing circuit connected to a positive pressure ventilator

Two modes of ventilation were tested using a Non-Invasive Positive Pressure Ventilator (model NIPPY3+, B&D Electromedical Ltd, Warwickshire, UK, Figs. 4(a) and 4(b)): *pressure support ventilation* and *intermittent positive pressure ventilation* (IPPV). The former may be used to achieve improved tidal volumes in spontaneously breathing patients who need assistance. The latter has been used to avoid intubation in patients with respiratory failure, to provide near-continuous ventilator support, improving oxygenation and decreasing hospital stay [14].

The set-up of the experiment using the ventilator was implemented with a heat and moisture exchanger (HME Anti-bacterial low resistance filter, B&D Electromedical Ltd, Warwickshire, UK) in the breathing circuit (Figs. 4(a) and 4(c)). The air outlet of the ventilator was connected to the humidification arm of the breathing circuit, providing active humidification by heating a water container (MR-850AEK, Fisher & Paykel Healthcare Limited, Berkshire, UK). The humidification arm was coupled with an exhalation valve which could be optionally connected to the HME. A T-valve linked the breathing circuit via a tube to a Lung Ventilator Performance Analyser (LVPA, previously marketed by BOC Medishield Ltd, Essex, UK).

The optical fibre sensor contained within a 23-gauge

medical hypodermic needle and capacitive sensor were both placed in the T-piece valve (Figs. 4(a) and 4(c)). There were also two removable temperature probes integrated in the breathing circuit, one included in the humidifier itself and another placed at the end of the humidification arm, just before the connection with the exhalation valve (see Fig. 4(a)). Independent of the mode of ventilation used, the change of humidity throughout the breathing circuit was controlled by switching on/off the humidifier. There are several classifications of HMEs: hydrophobic, hygroscopic, and filtered HMEs [4],[6]. In this case, a hygroscopic and filtered HME was used to reduce condensation in the T-piece (see left side of Fig. 4(c)) and the overall change of temperature inside the breathing circuit. The wool-foam material of this HME contains an anti-bacterial filter and hygroscopic chemicals (e.g. LiCl, $CaCl_2$) that reduces water condensation and the presence of moisture (small droplets), improving the response of the optical fibre humidity sensor.

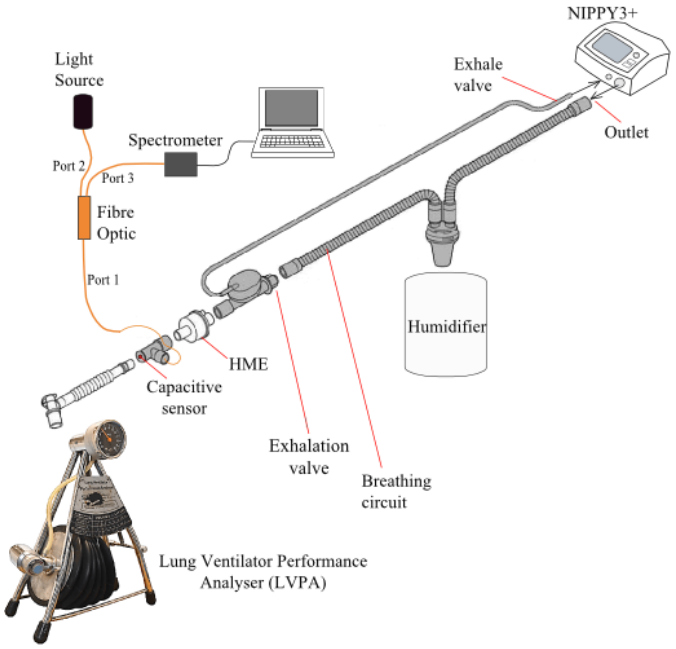

(a)

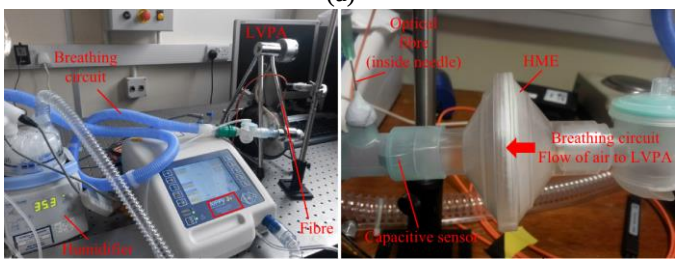

(b) (c)

Fig. 4. (a) Experimental set-up to measure the humidity level inside a breathing circuit connected to the ventilator. (b) Photograph of the experiment to measure humidity inside the breathing circuit connected to the non-invasive ventilator, without HME connected and the humidifier is based on heating the water container. (c) HME connected to the T-piece and exhalation valve of the breathing circuit.

III. Results

A. Sensor calibration

Fig. 5 shows the hydrophilic film (Figs. 5(b) and 5(c)) created during the LbL assembly process. Comparison of Fig. 5(b) and Fig. 5(c) confirms that highly uniform film is deposited onto optical fibre after 4 bilayers [15]. The growth of the initial layers is not uniform due to lack of surface coverage and some parts will not be fully charged after deposition of the first layers of PAH. Coverage can be boosted by controlling parameters such as solution concentration of the polyelectrolytes used, pH and dipping times [16]. More uniform multilayer growth has been reported with the use of an initial assembly adhesion stage of PAH and Poly(sodium 4-styrenesulfonate)(SPS) in the initial layers [17]. It should be noted that only the tip of the optical fibre coated with the PAH/SiO_2 film is interrogated and the side does not contribute to the sensor response.

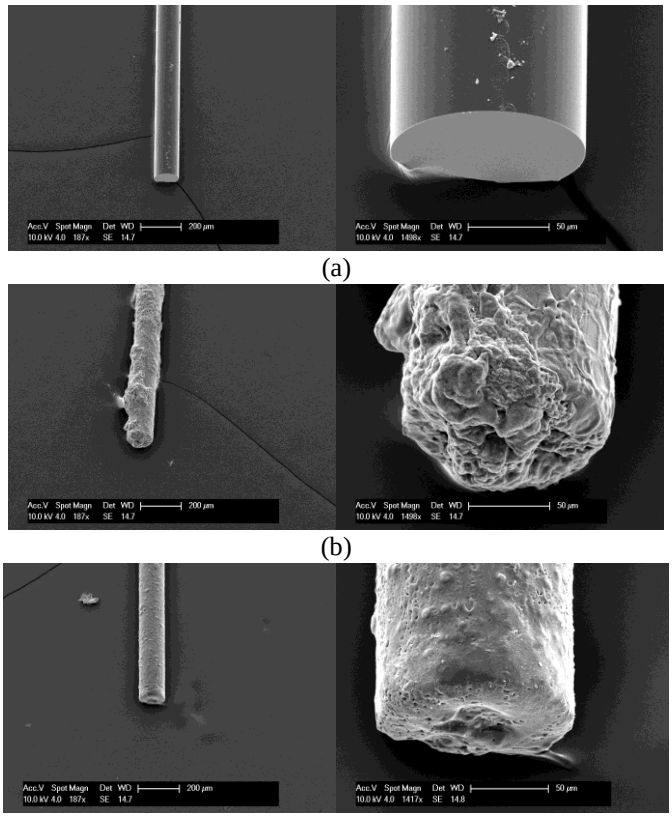

(a) (b) (c)

Fig. 5. Scanning Electron Microscope (SEM) images of the optical fibre humidity sensor probe coated with the PAH/SiO_2 film. (a) SEM image of the cleaved tip of an optical fibre without film. (b) SEM image of the fibre covered by 3 alternate bilayers of PAH and SiO_2 nanoparticles. (c) SEM image of the fibre covered by 5 alternate bilayers of same film. The scale bar on the left side is 200 μm; and 50 μm on the right hand side.

Fig. 6 shows a typical sensor response for a 4 bilayer film on exposure to different levels of humidity. The reflection spectra acquired are in the visible range and only the central wavelength (after applying a 100-points moving average filter) λ = 618.13 nm was plotted in all figures of this work in order to measure the response of the optical fibre humidity sensor. It

can be seen that the response of the optical fibre humidity sensor is inversely correlated with the response of the capacitive sensor. It should be noted that in this calibration experiment the temporal transitions of the capacitive sensor and optical fibre sensor between every step in Fig. 6, are similar and are only limited by the rate of change of air in the flowmeters, i.e. the transition times are not related to the response time of the two sensors.

Fig. 7 shows the effect of the film thickness on the sensitivity. The thicker PAH/SiO_2 film leads to an increase in the sensitivity of the optical fibre humidity sensor. The increase of the geometrical thickness leads to a sinusoidal-type change in the reflection (tracked at specific wavelengths) whose intensity depends on the number of layers [15], [18]. For three bilayers, the sensitivity was 0.26 mV/%RH, for four bilayers sensitivity increased to 0.53 mV/%RH and for nine bilayers, the sensitivity increased to 2.28 mV/%RH (Fig. 7). Briefly, the increase in the thickness of the film produces higher finesse values [19, Ch. 7] and therefore, sharper or more sensitive response to effective refractive index change (typically from 1.22 to 1.33) and geometrical thickness when the mesoporous film is exposed to water vapour molecules [8], [12].

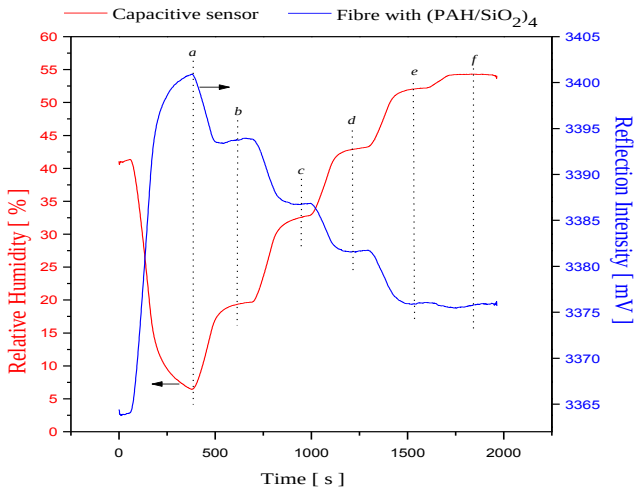

Fig. 6. Dynamic change of the optical fibre humidity sensor (response at λ = ca. 618.13 nm) modified with 4 bilayers thin film (blue line, $(PAH/SiO_2)_4$) upon exposure to the different levels of humidity. The red line is the RH change measured by the capacitive sensor. The average temperature is 25.4 ± 0.4 ℃ during all measurement of 30 min. The humidity levels produced with the flowmeters (Fig. 2(a)) are: (*a*) L_2=1 L/min, L_1=0 L/min; (*b*) L_2=0.8 L/min, L_1=0.2 L/min; (*c*) L_2=0.6 L/min, L_1=0.4 L/min; (*d*) L_2=0.4 L/min, L_1=0.6 L/min; (*e*) L_2=0.2 L/min, L_1=0.8 L/min; (*f*) L_2=0 L/min, L_1=1 L/min.

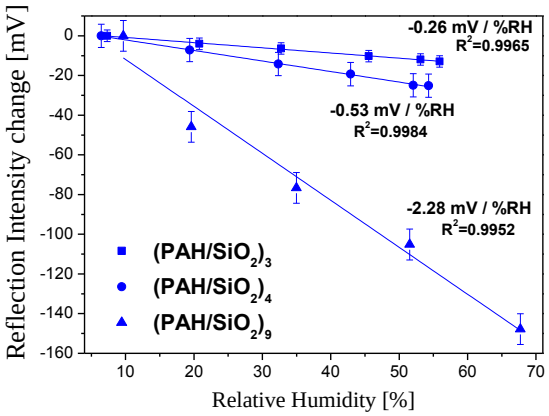

Fig. 7. Calibration curves for three, four and nine alternate bilayers of PAH/SiO_2 film showing the sensitivity for each case. For the purpose of clarity, the calibration curves are placed in the same plot showing differences in reflection intensity with respect to the first experimental value in each calibration curve.

In order to investigate the repeatability and hysteresis of the sensor, the optical fibre humidity probe with 9 bilayers was tested further using the set-up shown in Fig. 2(a). Through repeating three times in both forward from 5% RH to 76% RH (red line) and backward (blue line) directions, the hysteresis of the optical fibre humidity sensor with $(PAH/SiO_2)_9$ was obtained (Fig. 8). Finally, a least squares linear fit was performed on each calibration curve to obtain a sensitivity of 2.17mV/%RH and 2.28mV/%RH.

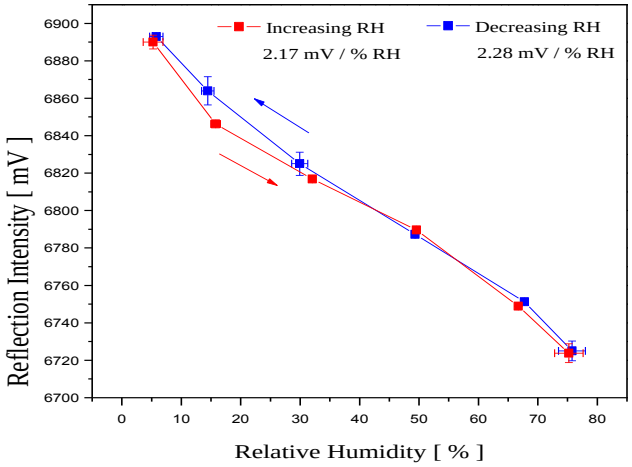

Fig. 8. Hysteresis of the optical fibre humidity sensor with 9 bilayers. The red trace is obtained by increasing the RH from 5% RH to 76% RH, and plotting reflection intensity measured in the fibre against RH measured in the capacitive sensor. The blue trace shows the decrease in RH from 76% RH to 5% RH.

B. Response time

Fig. 9 shows an example of a step response of the fibre sensor and capacitive sensor upon insertion into a humid environment. In this case, both sensors were simultaneously exposed (after 1800s) to environmental humidity through removing the Petri dish cover. The red trace corresponds to the

RH readings of the capacitive sensor, the blue trace the reflection intensity change in the fibre.

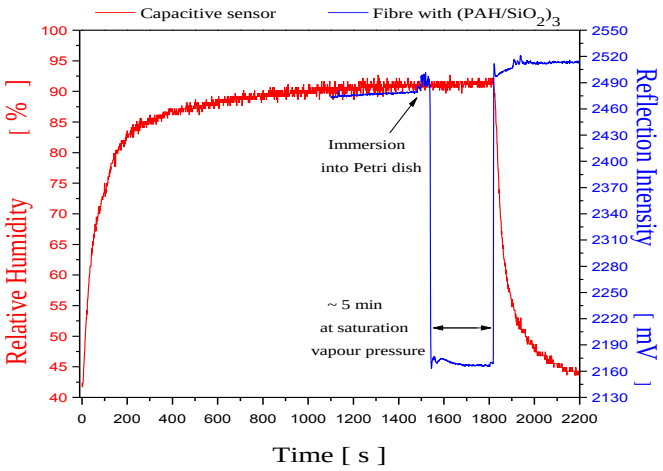

Fig. 9. Comparison of the response of the optical fibre humidity sensor with $(PAH/SiO_2)_3$ and the capacitive sensor. The red trace shows that the maximum humidity (92% RH) at saturation vapour pressure inside the Petri dish was reached after 20 min. The blue trace plots the response of the fibre sensor at saturation vapour pressure. At t = 1800 s, both the fibre sensor and the capacitive sensor were removed from the Petri dish and exposed to environmental humidity.

The mean response time of the optical fibre humidity sensor (based on the 1/e point) was 1.13 s with a standard deviation error of ± 0.30 s based on five measurements. The response time of the capacitive sensor is 158 seconds (five times longer than the time constant reported in the datasheet).

C. Non-invasive positive pressure ventilator breathing circuit tests

Fig. 10 shows the result of using the HME in the breathing circuit of the set-up presented in Fig. 4(a), demonstrating the pressure support mode of ventilation which is controlled by the breath of a patient except the pressure limit (in this case 20 cm H_2O). The step change in humidity is created by switching on the humidifier and later disconnecting the T-valve.

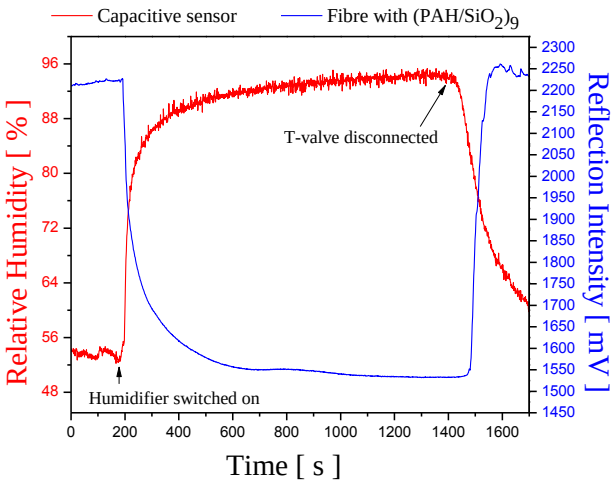

Fig. 10. Comparison of readings for 20 cm H_2O of pressure support mode and 101 L/min using HME in the breathing circuit. The red trace corresponds to the response of the capacitive sensor and the blue trace outputs the reflection intensity change of the optical fibre humidity sensor with 9 bilayers. The increase in humidity was caused by switching on the humidifier at 200 s and the decrease of humidity was produced by disconnecting the T-piece at 1500 s. The overall change of temperature (during all measurement of 1600 s) was 1.0 ℃ inside the T-piece.

Using the HME in the breathing circuit, the readings of the optical fibre humidity sensor (Fig. 10) are without artefacts produced mainly by formation of water condensation near the sensor and due to the presence of moisture (small droplets) that affect the fibre sensor performance (data not shown).

Fig. 11 shows measurements taken with the optical fibre humidity sensor with 9 bilayers and the capacitive sensor inside the T-piece of the breathing circuit (Figs. 4(a) and 4(c)) and using a different mode of ventilation, i.e. Intermittent Positive Pressure Ventilation (IPPV); this mode was first tested with a fixed pressure of 15 cm H_2O and 12 breaths per minute (Breaths/min) with the humidifier switched on. The output of a moving average filter (with 100 points) has been applied to the responses of the capacitive sensor and the optical fibre humidity sensor and the average baseline (black lines in Fig. 11) increased from 2968 mV to 3568 mV for the fibre sensor and decreased from 93%RH to 89%RH for the capacitive sensor during the measurement period (600s). The inset in Fig. 11 is a close up view between 200 and 260 seconds that corroborates that only the optical fibre humidity sensor can detect individual breaths due to its faster response.

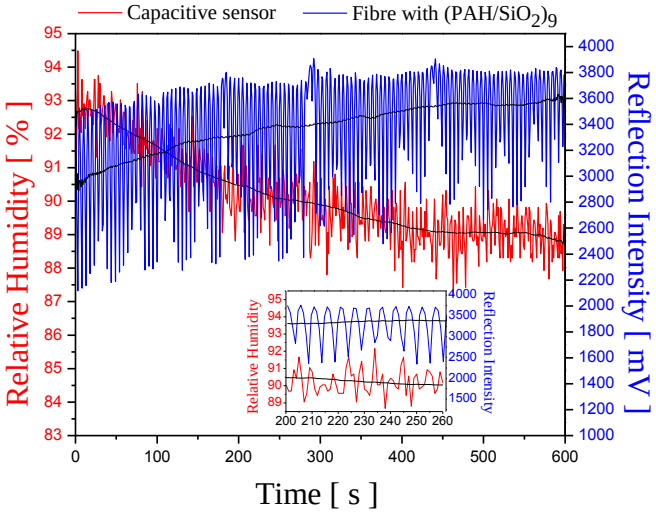

Fig. 11. Comparisons of 9 bilayer fibre response (blue trace) and capacitive sensor response (red trace) at 15 cm H_2O in IPPV mode and 12 Breaths/min; the black traces correspond to the output of a moving average filter for each device response. During the measurement period, the temperature increased from 28.2 to 30.7 ℃ in the T-piece. The inset presents a zoom from 200 s to 260 s of 15 cm H_2O in IPPV mode and 12 Breaths/min; the optical fibre is the only sensor capable of measuring individual breaths due to its faster response.

Figs. 12(a) and 12(b) show a new subset of measurements for t = 300 to 360s (600 s total experiment duration) with the optical fibre humidity sensor using 9 bilayers deposited on the

tip of the fibre. These measurements compare different breathing frequencies for the same pressure in IPPV mode and also compare different pressures of IPPV for the same frequency. The fast response of the sensor is again demonstrated through breath to breath humidity measurements. Fig. 12(a) confirms that the slower breath frequency will produce smaller baseline reflection intensity and higher RH for a fixed ventilation pressure of 30 cm H_2O. Fig. 12(b) shows that at lower pressures, IPPV will produce a smaller baseline reflection intensity and higher RH for a fixed breath frequency of 20 breaths/min.

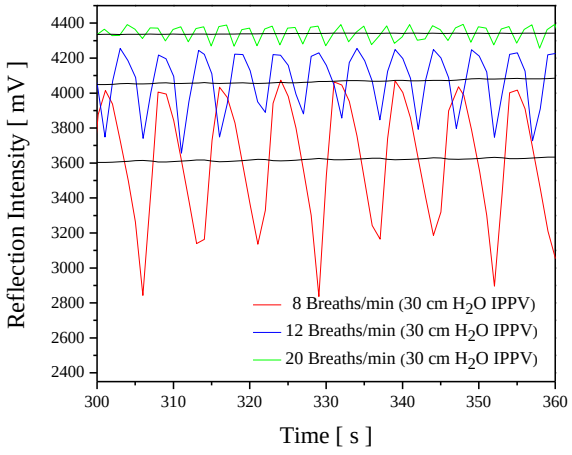

(a)

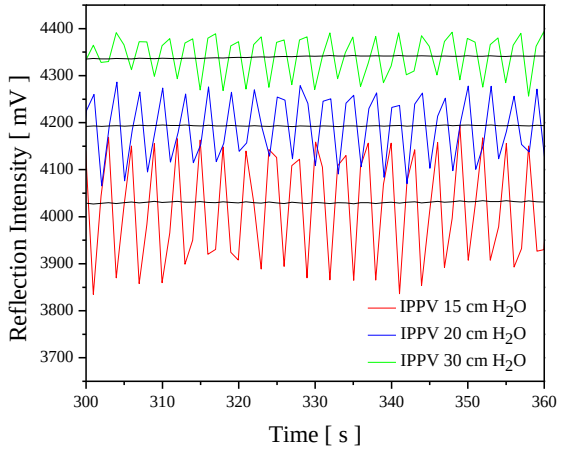

(b)

Fig. 12. (a) Comparison of different breaths/min for same pressure of IPPV; the behaviour shown is consistent for the whole experiment (600 s duration), i.e. independent of the level of humidity provided by the humidifier, a frequency of 8 breaths/min produced always a higher RH than 12 breaths/min and 20 breaths/min. (b) Comparison of different pressures of IPPV for the same frequency of breaths/min; the behaviour shown is consistent for the whole experiment (600s duration), the pressure of 15 cm H_2O always produced a higher RH than 20 cm H_2O and 30 cm H_2 O.

IV. Discussion

Although the fluctuations in the light source are small (drift less than 0.3% per hour), any transmission loss artefacts can be avoided by including a reference fibre without the mesoporous film in the system. In this way, any fluctuation in the light source and any other source of artefact (like motions in the sensor probe causing transmission losses) would be also detected by that reference fibre and could be significantly reduced through signal processing.

The results (section C) confirm that an HME acts as a hydrophobic filter protecting the sensor against condensation that can produce artefacts and is useful as it restricts temperature variations. In this direction, it is also beneficial to monitor temperature as it is well known that measuring relative humidity depends on temperature. The calibration results obtained in Figs. 6 to 9 were performed at a constant room temperature (23.0 ℃ ± 0.5 ℃). In practical use in non-invasive mechanical ventilation, large temperature variations can be avoided (up to ± 1 ℃) using an HME in the breathing circuit (Figs. 10 and 11). In future, it would also be favourable to coat the tip of the hypodermic needle containing the fibre-optic sensor with the wool/foam material used in the HME and further improvements could be made by writing a fibre Bragg grating into the fibre so that temperature can be simultaneously monitored. The main reason to use the spectrometer in this paper was to optimize the working wavelength and this could be simplified using an LED and photodetector. However as future work will involve the use of fibre Bragg gratings to monitor temperature it is likely that the spectrometer will be retained.

Future work will investigate how the response time and sensitivity change with SiO_2 nanoparticle size, optimizing levels of aggregation and porosity. Surface coverage of the initial layers onto the tip of the optical fibre can be also improved by modifying the deposition procedure and increasing the efficiency of SiO_2 adsorption through direct surface modification of the nanoparticles (creating higher number of ligands that will intensify the negative charge of the SiO_2 particles before they are coated with PAH).

V. Conclusions

The sensitivity, response time and hysteresis of a novel optical fibre humidity sensor, based on Fabry-Perot interferometric sensing, has been investigated over a humidity range of 5% RH and 76% RH using a controlled bench-top set-up. The performance was also evaluated in the breathing circuit of a mechanical ventilator. The sensor response allows measurement levels of humidity near 100% RH in the Y-piece of the circuit in an invasive ventilator or in the T-piece of a non-invasive ventilator.

The sensitivity of the optical fibre humidity sensor increased with the number of bilayers with a maximum sensitivity of 2.28 mV/%RH obtained with 9 bilayers (~450 nm overall thickness film). The response time constant of the optical fibre humidity sensor was 1.13 ± 0.3 s compared to the measured 158 s response rate for a commercial capacitive sensor under the same experiment conditions. The optical fibre humidity sensor proposed has a very simple and low cost

porous structured sensing element obtained with PAH/SiO_2 using the LbL fabrication method. The results demonstrate low hysteresis with a response time within current fast trends reported in recent reviews on optical humidity sensors.

The fast response of the sensor means that it is possible to track humidity changes in an individual's respiratory rate (or presence/absence of breathing) during mechanical ventilation. All the components of the optical sensor require no electrical current, are non-magnetic materials, and so the device could be used during magnetic resonance imaging, oncological treatments or during anaesthesia. Future work will investigate the applications of this sensor in volunteers, and a variety of patient groups.

The results demonstrate that the development of a portable optical fibre humidity sensor is feasible and can be easily embedded in ventilation masks or in elements of the breathing circuits used for ventilation.

ACKNOWLEDGMENT

The authors want to thank the support of the Invention for Innovation Programme (NIHR i4i II-LA-0813-20008) of the National Institute of Health Research (NIHR, UK). FUH acknowledges the support of the National Council of Science and Technology of Mexico (CONACyT) and the Ministry of Public Education in Mexico (DGRI-SEP) for a scholarship. The authors also want to thank Dr. Rishie Sinha for his constructive comments in the preparation of this manuscript.

REFERENCES

[1] T. Williams, "Humidification in intensive care," *SAJCC*, vol. 21, no. 1, pp. 26-31, July 2005.

[2] A. M. Esquinas Rodriguez et al., "Clinical Review: Humidifiers during non-invasive ventilation - key topics and practical implications," *Crit. Care*, vol. 16, no. 203, pp. 1-7, Feb. 2012.

[3] S. A. Kolpakov et al., "Toward a new generation of photonic humidity sensors," *Sensors*, vol. 14, pp. 3986-4013, Feb. 2014.

[4] J.K. Zuur et al., "The physiological rationale of heat and moisture exchangers in post-laryngectomy rehabilitation: a review," *Eur. Arch. Otorhinolaryngol*., vol. 263, pp. 1-8, Jan. 2006.

[5] J. K. Zuur et al., "A newly developed tool for intra-tracheal temperature and humidity assessment in laryngectomized individuals: the Airway Climate Explorer (ACE)," *Med. Bio. Eng. Comput.*, vol. 45, pp. 737-745, July 2007.

[6] R. D. Restrepo and B. K. Walsh, "Humidification during invasive and noninvasive mechanical ventilation: 2012," *Respir. Care*, vol. 57, no. 5, pp. 782-788, May 2012.

[7] L. Lorente et al., "Ventilator-associated pneumonia using a heated humidifier or a heat and moisture exchanger: a randomized controlled trial," *Crit. Care*, vol. 10, no. 4, pp. 1-7, Aug. 2006.

[8] J. S. Santos et al., "Characterisation of a Nafion film by optical fibre Fabry-Perot interferometry for humidity sensing," *Sensor Actuat. B-Chemical*, vol. 196, pp. 99-105, Jan. 2014.

[9] L. Alwis et al., "Optical fibre-based sensor technology for humidity and moisture measurement: Review of recent progress," *Measurement*, vol. 46, pp. 4052-4074, July 2013.

[10] Z. L. Ran et al., "Laser-micromachined Fabry-Perot optical fiber tip sensor for high resolution temperature-independent measurement of refractive index," *Opt. Express*, vol. 16, no. 3, pp. 2252-2263, Feb. 2008.

[11] C. Huang et al., "Optical fiber humidity sensor with porous $TiO_2/SiO_2/TiO_2$ coatings on fiber tip," *IEEE Photon. Technol. Lett.*, vol. 27, no. 14, pp. 1495-1498, July 2015.

[12] J. M. Corres et al., "Optical fiber humidity sensors using nanostructured coatings of SiO2 nanoparticles," *IEEE Sensors J.*, vol. 8, no. 3, pp. 281-285, Mar. 2008.

[13] M.K. Chakrabarti and M.K. Sykes, "Evaluation of the lung ventilator performance analyser," *Anaesthesia*, vol. 31, pp. 521-528, May 1976.

[14] P. Leger et al., "Nasal intermittent positive pressure ventilation. Long-term follow-up in patients with severe chronic respiratory insufficiency," *CHEST*, vol. 105, no. 1, pp. 100-105, Jan. 1994.

[15] I. Del Villar et al., "Fiber-Optic hydrogen peroxide nanosensor," *IEEE Sensors J.*, vol. 5, no. 3, pp. 365-371, June 2005.

[16] V. Mohanta and S. Patil, "Enhancing surface coverage and growth in layer-by-layer assembly of protein nanoparticles," *Langmuir*, vol. 29. no. 43, pp. 13123-13128, Aug. 2013

[17] J. Bravo et al., "Transparent superhydrophobic films based on silica nanoparticles," *Langmuir*, vol. 23, no. 13, pp. 7293-7298, Jan. 2007.

[18] F. J. Arregui et al., "Optical fiber nanometer-scale Fabry-Perot interferometer formed by the ionic self-assembly monolayer process," *Opt. Lett.*, vol. 24, no. 9, pp. 596-598, May 1999.

[19] B. E. A. Saleh and M. C. Teich, "Photonic-crystal optics," in *Fundamentals of Photonics*, 2nd ed. Boston, Massachusetts: Wiley-Interscience, 2007, Ch. 7, sec. 7.1, pp. 243-264.